The Kapowski Chronicles: A Complete, Volumetric Cortical Thickness Open Source Pipeline with Evaluation on Public Data

Nicholas J. Tustison[†a,1], Brian B. Avants[†b], Philip A. Cook[b], Gang Song[b], Sandhitsu R. Das[b], Jeffrey R. Duda[b], Niels van Strien[c], James R. Stone[a], James C. Gee[b]

[a]*Department of Radiology and Medical Imaging, University of Virginia, Charlottesville, VA*
[b]*Penn Image Computing and Science Laboratory, University of Pennsylvania, Philadelphia, PA*
[c]*Department of Circulation and Medical Imaging, Norwegian University of Science and Technology, Trondheim, Norway*

Abstract

Numerous studies have explored the relationship between cortical structure and brain development, cognitive function and functional connectivity. The highly convoluted cortical topography makes manual measurements arduous and often impractical given the population sizes necessary for sufficient statistical power. Computational techniques have permitted large-scale studies as they provide robust and reliable localized measurements characterizing the cortex with little or no human intervention. Particularly useful to the neuroscience community are publicly available tools, such as the popular surface-based Freesurfer, which facilitate the testing and refinement of hypotheses. In this paper, we introduce the volume-based Advanced Normalization Tools (ANTs) cortical thickness automated pipeline comprising well-vetted components such as SyGN (multivariate template construction), SyN (image registration), N4 (bias correction), Atropos (*n*-tissue segmentation), and DiReCT (cortical thickness) all developed as part of the ANTs open science effort. Complementing the open source aspect of ANTs we confirm previous findings of gender differences, age correlation, and hemispherical asymmetry in cortical thickness using the publicly available IXI data consisting of multimodal structural MRI of approximately 600 subjects. To further promote open science and use of the proposed tools, all scripts and templates used to produce the results are hosted on the Neuroimaging Informatics Tools and Resources Clearinghouse (NITRC) website.

Keywords: advanced normalization tools, bias correction, cortical thickness, open source software, segmentation, skull stripping

1. Introduction

Historically rooted in the meticulous work of von Economo [22], imaging-based structural analysis of the brain plays a fundamental role in identifying the relationship between cortical morphology, disease and cognition. Quantitative cortical measures are able to identify abnormalities in such conditions as Huntington's disease [57, 56, 60], schizophrenia [50], bipolar disorder [45], Alzheimer's disease and frontotemporal dementia [21, 19], Parkinson's disease [36], Williams syndrome [70], multiple sclerosis [55], autism [12, 33], migraines [17], chronic smoking [41], alcoholism [29], cocaine addiction [48], Tourette syndrome in children [68], scoliosis in female adolescents [73], obsessive compulsive disorder [64], ADHD [1], obesity [54], and heritable [52] and elderly [8] depression. Cortical thickness also varies normally as a function of age [39], gender [44], untreated transsexuality [80], handedness [43, 2], intelligence [63], athletic ability [75], musical ability [9, 30], tendency toward criminality [53], and Tetris-playing ability in female adolescents [32]. Additionally, recent studies demonstrate possible functional connectivity relationships using cortical thickness measures [76, 42, 34]. Although these findings are subject to debate and interpretation [31], the availability of quantitative computational methods for extracting such information has proven invaluable for developing and refining fundamental neuroscience hypotheses.

Computational methods for analyzing the cortex may be broadly characterized as surface mesh-based or volumetric [58, 13]. Representative of the former is the Freesurfer[2] cortical modeling software package [15, 27, 25, 26, 28] which owes its popularity to public availability, excellent documentation, good performance, and integration with other toolkits, such as the extensive FMRIB software library (FSL) [67]. Similar to other surface approaches (e.g. [18, 47, 46, 37]), the pial and white matter surfaces from individual subject MR data are modeled with polygonal meshes which are then used to determine local cortical thickness based on a specified correspondence between the surface models.

Image volumetric (or meshless) techniques vary both in algorithmic terms as well as the underlying definition of cortical thickness. An early, foundational technique is the method of [35] in which the inner and outer surface geometry is used to determine the solution to Laplace's equation where thickness is measured by integrating along the tangents of the resulting field lines spanning the boundary surfaces. Subsequent contributions

[1]Corresponding author: PO Box 801339, Charlottesville, VA 22908; T: 434-924-7730; email address: ntustison@virginia.edu.

†The first two authors contributed equally to this work.

[2]http://surfer.nmr.mgh.harvard.edu/

improved upon the original formulation. For example, in [77], an Eulerian PDE approach was proposed to facilitate the computation of correspondence paths. Extending the surface-based work of [46], the hybrid approach of [37] uses the discrete Laplacian field to deform the white matter surface mesh towards the pial surface. Although the Laplacian-based approach has several advantages including generally lower computational times and non-crossing correspondence paths, direct correlative assessments with histology are potentially problematic as the quantified distances are not necessarily Euclidean. Other volumetric algorithms employ coupled level sets [78], model-free intelligent search strategies either normal to the gray-white matter interface [58] or using a min-max rule [72]. Most relevant to this work is the DiReCT (Diffeomorphic Registration-based Cortical Thickness) algorithm proposed by [16] in which a registration-based approach proposed where the derived diffeomorphic mapping between the white and pial matter surfaces is used to propagate thickness values through the cortical gray matter. A unique benefit of DiReCT is that it naturally estimates the boundaries of buried sulci by employing a diffeomorphic constraint on the probabilistic estimate of the gray matter and cerebrospinal fluid interface.

Despite the variety of techniques for estimating cortical thickness from imaging data (of which only a fraction are cited), several common pre-processing components may be identified. The most fundamental of these include inhomogeneity correction, skull stripping, and *n*-tissue segmentation for differentiating the gray and white matter. For statistical analysis across large populations, construction of population-specific unbiased templates is also beneficial [23]. In addition, some of these steps might include a crucial registration component, e.g. propagating template-based tissue priors for improved segmentation. The requisite additional components coupled with the general lack of availability of published algorithms [40] inhibits performing studies by external researchers and makes comparative evaluations difficult. For example, one recent evaluation study [13] compared Freesurfer (a surface-based method) with two volumetric methods [35, 16]. Whereas the entire Freesurfer processing pipeline has been made publicly available, tuned by the original authors in terms of implementation, and described in great detail (specifically in terms of suggested parameters); both volumetric methods were implemented solely by the authors of the evaluation (not the actual algorithmic developers) using unspecified parameters making the comparisons less than ideal. Further complicating comparisons is distinct processing domains between volumetric and surface-based techniques and the potential for the introduction of bias [38].

In this work, we describe our Insight Toolkit (ITK)-based cortical thickness pipeline which is freely available as part of the Advanced Normalization Tools (ANTs) software package. This includes all the necessary preprocessing steps consisting of well-vetted previously published algorithms for bias correction [71], brain extraction [4], *n*-tissue segmentation [6], template construction [7], and image normalization [5]. We also describe improvements made to the original DiReCT algorithm [16]. Equally as important, we provide explicit coordination between these pipeline components complete with a set of useful parameters which are employed to analyze the publicly available IXI data set. The full pipeline and parameter set is encapsulated in a well-documented shell script which is also available in ANTs. Furthermore, we provide all the derived image data and other processing scripts on the NITRC repository specifically meant for this publication. The availability of both the code and data permits the set of results described in this work to be fully reproducible. This permits other researchers to contrast their own results against this baseline processing and to adapt the given volumetric pipeline for measuring cortical thickness with their own datasets.

2. Methods and Materials

2.1. ANTs volumetric-based cortical thickness estimation pipeline

The ANTs-based cortical thickness estimation workflow is illustrated in Figure 1. The steps are as follows:

1. initial N4 bias correction on input anatomical MRI,
2. brain extraction using a hybrid segmentation/template-based strategy,
3. alternating between prior-based segmentation and white matter posterior probability weighted bias correction,
4. DiReCT-based cortical thickness estimation, and
5. optional normalization to specified template.

Each component, including both software and data, is briefly detailed below with the relevant references for additional information.

Additionally, the coordination of all the algorithmic components is encapsulated in the shell script `antsCorticalThickness.sh`. This includes optimal parameters for each of the algorithmic components which has worked well for our processing and which are used to acquire the results described in this work.

2.1.1. Anatomical template construction

Normalizing images to a standard coordinate system reduces intersubject variability in population studies. Various approaches exist for determining the normalized space such as the selection of a pre-existing template based on a single subject, e.g. the Talairach atlas [69], or a publicly available averaged group of subjects, e.g. the MNI [14] or ICBM [49] templates. Additionally, mean templates constructed from labeled data can be used to construct spatial priors for improving segmentation algorithms. The work of [7] explicitly models the geometric component of the normalized space during optimization to produce such mean templates. Coupling the intrinsic symmetry of SyN pairwise registration [5] and an optimized shape-based sharpening/averaging of the template appearance, Symmetric Group Normalization (SyGN) is a powerful framework for producing optimal population-specific templates [7] with arbitrary similarity metric choice.

The ANTs implementation of this technique is currently available as a shell script,

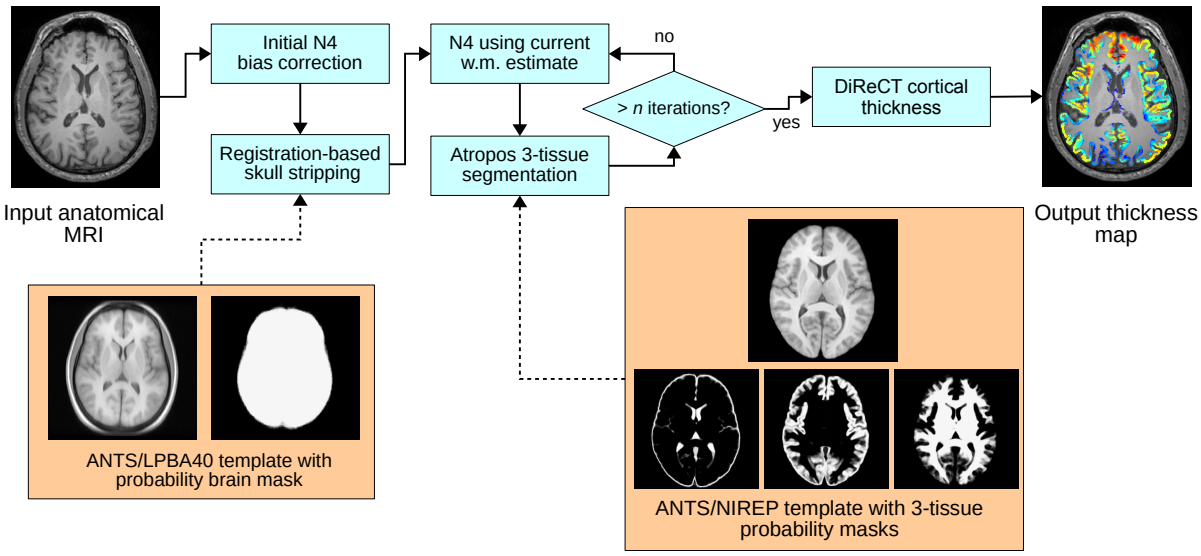

Figure 1: The ANTs T1 processing workflow containing all elements for determining cortical thickness. Not shown is the optional single subject to template registration.

`buildtemplateparallel.sh`, and a multivariate version, `antsMultivariateTemplateConstruction.sh`, both of which are distributed as part of the ANTs repository. The latter script permits the construction of multimodal templates (e.g. T1-weighted, T2-weighted, and proton density MRI as described in the Evaluation section). Both scripts accommodate a variety of computational resources for facilitating template construction. These computational resource possibilities include:

- serial processing on a single workstation,
- parallelized processing on a single workstation with multiple cores using `pexec`[3],
- parallelized processing using Apple's XGrid technology[4],
- parallelized processing using Sun Grid Engine for cluster-based systems[5], and
- parallelized processing using the Portable Batch System for cluster-based systems[6].

Within this work multiple templates were created for all stages of image processing and analysis. The creation of these templates are described in the corresponding data section.

what is the motivation of the multivar template here? it would seem useful to add an FA component to the segmentation step to aid in cortical / wm delineation which would motivate the multivar template approach but might be difficult to establish that this actually helps .... though we could compare both ways : univar and multivar

2.1.2. *N4 Bias field correction*

Critical to quantitative processing of MRI is the minimization of field inhomogeneity effects which causes artificial low frequency intensity variation across the image. Large-scale studies, such as the Alzheimer's Disease Neuroimaging Initiative (ADNI), employ perhaps the most widely used bias correction algorithm, N3 [65], as part of their standard protocol [10].

In [71], we introduced an extension of N3, denoted as N4, which demonstrates improved performance and convergence behavior on a variety of data. This improvement is a result of an enhanced fitting routine (which includes multi-resolution capabilities) and a modified optimization formulation. For our workflow, the additional possibility of specifying a weighted mask in N4 permits the use of the current white matter probability map calculated during the segmentation pipeline for further improvement of bias field estimation. In addition to its public availability through ANTs and the Insight Toolkit, it has also been included in the popular open source Slicer software package for visualization and medical image computing [24].

N4 is used in two places during the individual subject processing (cf. Figure 1). Following conversion of the raw dicom T1-weighted image to Nifti format using our related `Neuropipedream` set of raw image conversion and organization tools[7], N4 is used to generate an initial bias corrected image for use in brain extraction. The input mask is created by adaptively thresholding the background from the foreground using

[3] http://www.gnu.org/software/pexec/pexec.1.html
[4] https://developer.apple.com/hardwaredrivers/hpc/xgrid_intro.html
[5] http://www.oracle.com/technetwork/oem/grid-engine-166852.html
[6] http://www.pbsworks.com/
[7] http://sourceforge.net/projects/neuropipedream/

Otsu's algorithm [51]. Following brain extraction, the three-tissue segmentation involves iterating between bias field correction using the current white matter posterior probability as a weight mask and then using that bias corrected image as input to the Atropos segmentation step (described in subsequent sections).

2.1.3. Atropos 3-tissue segmentation

In [6] we presented an open source n-tissue segmentation software tool (which we denote as "Atropos") attempting to distill 20+ years of active research in this area particularly some of its most seminal work (e.g. [79, 3]). Specification of prior probabilities includes spatially varying Markov Random Field modeling, prior label maps, and prior probability maps typically derived from our template building process. Additional capabilities include handling of multivariate data, partial volume modeling [62], a memory-minimization mode, label propagation, a plug-n-play architecture for incorporation of novel likelihood models which includes both parametric and non-parametric models for both scalar and tensorial images, and alternative posterior formulations for different segmentation tasks.

In order to better integrate Atropos and N4, we use a pure tissue probability weight mask generated from the posterior probabilities generated by the segmentation process. Given N labels and the corresponding N posterior probability maps $\{P_1, \ldots, P_N\}$ produced during the segmentation process, the N4 weight mask is created at each N4 $\Leftrightarrow$ Atropos iteration from:

$$P_{pure\ tissue}(\mathbf{x}) = \sum_{i=1}^{N} P_i(\mathbf{x}) \prod_{j=1, j\neq i}^{N} \Big(1 - P_j(\mathbf{x})\Big). \qquad (1)$$

2.1.4. Brain extraction

Brain extraction using ANTs combines template building, high-performance brain image registration [5], and Atropos with topological refinements. An optimal template for brain extraction is generated offline using labeled brain data. For example, in this work we use the LPBA40 data for generating a brain extraction template and a corresponding brain probability mask which is available on the website associated with this submission.

The warped template probability map is thresholded at 0.5 and the resulting mask is dilated with a radius of 2. Atropos is used to generate an initial 3-tissue segmentation estimate within the mask region. Each of the three tissue masks undergo specific morphological operations which are then combined to create a brain extraction mask for use in the rest of the cortical thickness workflow. does there need to be a bit more technical detail here? while you can refer to the script, why perform these operations? there are numerous references, most germane probably some recent stuff from J Prince (i think) and the freesurfer watershed approach which came from ... i forget ... maybe one of the french groups.

A comparison using open access brain data with publicly available brain extraction algorithms including AFNI's `3dIntracranial` [74], FSL's `BET2` [66], Freesurfer's `mri_watershed` [59], and BrainSuite [20] demonstrated that our combined registration/segmentation approach [4] performs at the top level alongside BrainSuite (tuned) and FreeSurfer. ok you have the segonne ref here ...

2.1.5. DiReCT Cortical Thickness Estimation

Although the basic formulation of DiReCT as reported in this work is as it was introduced in [16], we have made several improvements. Perhaps the most significant advance is that this particular ITK-compatible implementation has been significantly multi-threaded, is written in ITK coding style, and has been made publicly available through ANTs complete with a unique user interface design developed specifically for ANTs tools.

2.2. Public Data Resources

2.2.1. LPBA40 Data for Skull Stripping

For the brain extraction step we used the data from the LPBA40 repository [61]. These data consist of 40 high-resolution 3D Spoiled Gradient Echo (SPGR) MRI acquisitions which were manually labeled delineating 56 brain structures. Additional post processing included automated brain extraction using FSL's brain extraction tool [66] which was followed by manual corrections. These 40 brain masks are also included with the database.

All 40 subjects were used to create a population-specific unbiased average template [7]. The brain masks corresponding to the 20 subjects were warped to the template space using the transforms derived during the template building process. A template probability mask was created by averaging the warped brain masks. For brain extraction of any single individual this ANTS-based LPBA40 template is coarsely registered to the single subject brain. The template probability brain mask is warped to the individual subject and is used as the initial brain mask estimate. As mentioned previously, Atropos and binary morphological operations are used to refine the brain mask estimate.

2.2.2. NIREP Data for 3-Tissue Segmentation

The nonrigid image registration evaluation project is an ongoing framework for evaluating image registration algorithms [11]. The initial data set introduced into the project consists of 16 (8 male and 8 female) high resolution skull-stripped brain data with 32 cortical labels (cf Table 1) manually drawn using a published protocol.[8] Given the gray matter labels, the white matter and CSF were identified for each of the 16 subjects using Atropos. Similar to the LPBA40 data set, a NIREP template was created from all 16 subjects and each of the warped labels were used to create probabilistic estimates of the labeled region boundaries. These probability maps were used as spatial prior probabilities during the 3-tissue segmentation component of the pipeline. Using SyN, the NIREP template is registered to the extracted individual subject brain which is followed by a

[8] http://www.nirep.org/

1) L occipital lobe	2) R occipital lobe
3) L cingulate gyrus	4) R cingulate gyrus
5) L insula gyrus	6) R insula gyrus
7) L temporal lobe	8) R temporal lobe
9) L superior temporal gyr.	10) R superior temporal gyr.
11) L infero temporal region	12) R infero temporal region
13) L parahippocampal gyr.	14) R parahippocampal gyr.
15) L frontal pole	16) R frontal pole
17) L superior frontal gyrus	18) R superior frontal gyrus
19) L middle frontal gyrus	20) R middle frontal gyrus
21) L inferior gyrus	22) R inferior gyrus
23) L orbital frontal gyrus	24) R orbital frontal gyrus
25) L precentral gyrus	26) R precentral gyrus
27) L superior parietal lobule	28) R superior parietal lobule
29) L inferior parietal lobule	30) R inferior parietal lobule
31) L postcentral gyrus	32) R postcentral gyrus

Table 1: The 32 cortical NIREP labels.

warping of the NIREP priors to the space of the individual subject. The initial warped white matter probability map is used as the weighted confidence mask in the follow-up bias correction step.

2.3. IXI Data for Pipeline Evaluation

The IXI data[9] used for the evaluation consists of 577 healthy subjects imaged at three sites using several modalities (T1-weighted, T2-weighted, proton density, magnetic resonance angiography, and diffusion tensor imaging). The database also consists of demographic information such as age, weight, height, ethnicity, occupation category, educational level, and marital status. The number of subjects spanning a range of demographic characteristics makes this a rich data set for validating and exploring correlations with cortical thickness measured using the ANTs pipeline.

3. Discussion and Conclusions

Acknowledgments

References

[1] Almeida Montes, L. G., Prado Alcántara, H., Martínez García, R. B., De La Torre, L. B., Avila Acosta, D., Duarte, M. G., Mar 2012. Brain cortical thickness in ADHD: Age, sex, and clinical correlations. J Atten Disord.

[2] Amunts, K., Armstrong, E., Malikovic, A., Hömke, L., Mohlberg, H., Schleicher, A., Zilles, K., Feb 2007. Gender-specific left-right asymmetries in human visual cortex. J Neurosci 27 (6), 1356–64.

[3] Ashburner, J., Friston, K. J., Jul 2005. Unified segmentation. Neuroimage 26 (3), 839–51.

[4] Avants, B. B., Klein, A., Tustison, N. J., Woo, J., Gee, J. C., 2010. Evaluation of an open-access, automated brain extraction method on multi-site multi-disorder dat. Human Brain Mapping.

[5] Avants, B. B., Tustison, N. J., Song, G., Cook, P. A., Klein, A., Gee, J. C., Feb 2011. A reproducible evaluation of ANTs similarity metric performance in brain image registration. Neuroimage 54 (3), 2033–44.

[9] http://biomedic.doc.ic.ac.uk/brain-development/

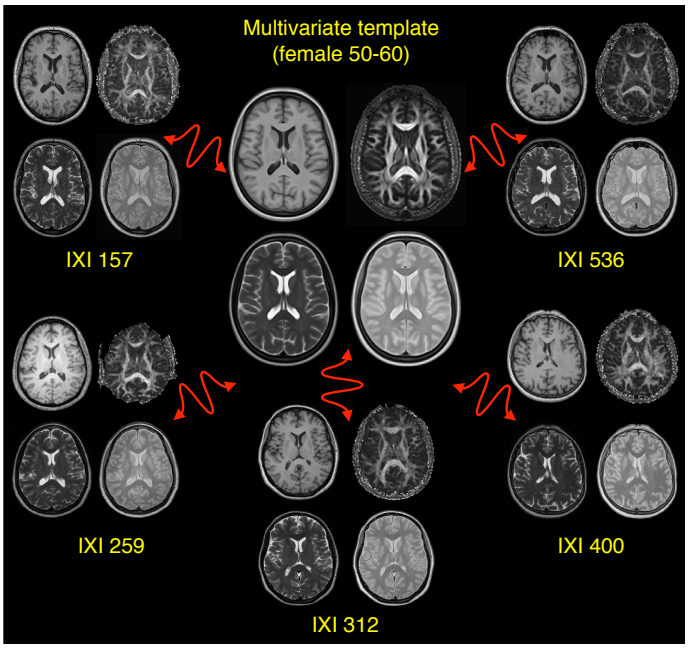

Figure 2: Sample multivariate template constructed from a subset of the IXI data (female, age 50–60). Axial slices of five of the 37 total subjects from this cohort are shown.

[6] Avants, B. B., Tustison, N. J., Wu, J., Cook, P. A., Gee, J. C., Dec 2011. An open source multivariate framework for *n*-tissue segmentation with evaluation on public data. Neuroinformatics 9 (4), 381–400.

[7] Avants, B. B., Yushkevich, P., Pluta, J., Minkoff, D., Korczykowski, M., Detre, J., Gee, J. C., Feb 2010. The optimal template effect in hippocampus studies of diseased populations. Neuroimage 49 (3), 2457–66.

[8] Ballmaier, M., Sowell, E. R., Thompson, P. M., Kumar, A., Narr, K. L., Lavretsky, H., Welcome, S. E., DeLuca, H., Toga, A. W., Feb 2004. Mapping brain size and cortical gray matter changes in elderly depression. Biol Psychiatry 55 (4), 382–9.

[9] Bermudez, P., Lerch, J. P., Evans, A. C., Zatorre, R. J., Jul 2009. Neuroanatomical correlates of musicianship as revealed by cortical thickness and voxel-based morphometry. Cereb Cortex 19 (7), 1583–96.

[10] Boyes, R. G., Gunter, J. L., Frost, C., Janke, A. L., Yeatman, T., Hill, D. L. G., Bernstein, M. A., Thompson, P. M., Weiner, M. W., Schuff, N., Alexander, G. E., Killiany, R. J., DeCarli, C., Jack, C. R., Fox, N. C., ADNI Study, Feb 2008. Intensity non-uniformity correction using N3 on 3-T scanners with multichannel phased array coils. Neuroimage 39 (4), 1752–62.

[11] Christensen, G. E., Geng, X., Kuhl, J. G., Bruss, J., Grabowski, T. J., Pirwani, I. A., Vannier, M. W., Allen, J. S., Damasio, H., 2006. Introduction to the non-rigid image registration evaluation project (NIREP). In: Proceedings of the Third international conference on Biomedical Image Registration. WBIR'06. Springer-Verlag, Berlin, Heidelberg, pp. 128–135.

[12] Chung, M. K., Robbins, S. M., Dalton, K. M., Davidson, R. J., Alexander, A. L., Evans, A. C., May 2005. Cortical thickness analysis in autism with heat kernel smoothing. Neuroimage 25 (4), 1256–65.

[13] Clarkson, M. J., Cardoso, M. J., Ridgway, G. R., Modat, M., Leung, K. K., Rohrer, J. D., Fox, N. C., Ourselin, S., Aug 2011. A comparison of voxel and surface based cortical thickness estimation methods. Neuroimage 57 (3), 856–65.

[14] Collins, D. L., Neelin, P., Peters, T. M., Evans, A. C., 1994. Automatic 3D intersubject registration of MR volumetric data in standardized Talairach space. J Comput Assist Tomogr 18 (2), 192–205.

[15] Dale, A. M., Fischl, B., Sereno, M. I., Feb 1999. Cortical surface-based analysis. i. segmentation and surface reconstruction. Neuroimage 9 (2), 179–94.

[16] Das, S. R., Avants, B. B., Grossman, M., Gee, J. C., Apr 2009. Registration based cortical thickness measurement. Neuroimage 45 (3), 867–79.

[17] DaSilva, A. F. M., Granziera, C., Snyder, J., Hadjikhani, N., Nov 2007.

Thickening in the somatosensory cortex of patients with migraine. Neurology 69 (21), 1990–5.

[18] Davatzikos, C., Bryan, N., 1996. Using a deformable surface model to obtain a shape representation of the cortex. IEEE Trans Med Imaging 15 (6), 785–95.

[19] Dickerson, B. C., Bakkour, A., Salat, D. H., Feczko, E., Pacheco, J., Greve, D. N., Grodstein, F., Wright, C. I., Blacker, D., Rosas, H. D., Sperling, R. A., Atri, A., Growdon, J. H., Hyman, B. T., Morris, J. C., Fischl, B., Buckner, R. L., Mar 2009. The cortical signature of Alzheimer's disease: regionally specific cortical thinning relates to symptom severity in very mild to mild AD dementia and is detectable in asymptomatic amyloid-positive individuals. Cereb Cortex 19 (3), 497–510.

[20] Dogdas, B., Shattuck, D. W., Leahy, R. M., Dec 2005. Segmentation of skull and scalp in 3-D human MRI using mathematical morphology. Hum Brain Mapp 26 (4), 273–85.

[21] Du, A.-T., Schuff, N., Kramer, J. H., Rosen, H. J., Gorno-Tempini, M. L., Rankin, K., Miller, B. L., Weiner, M. W., Apr 2007. Different regional patterns of cortical thinning in Alzheimer's disease and frontotemporal dementia. Brain 130 (Pt 4), 1159–66.

[22] Economo, C., Koskinas, G. N., Triarhou, L. C., 2008. Atlas of cytoarchitectonics of the adult human cerebral cortex, 1st Edition. Karger, Basil.

[23] Evans, A. C., Janke, A. L., Collins, D. L., Baillet, S., Aug 2012. Brain templates and atlases. Neuroimage 62 (2), 911–22.

[24] Fedorov, A., Li, X., Pohl, K. M., Bouix, S., Styner, M., Addicott, M., Wyatt, C., Daunais, J. B., Wells, W. M., Kikinis, R., 2011. Atlas-guided segmentation of vervet monkey brain MRI. Open Neuroimag J 5, 186–97.

[25] Fischl, B., Dale, A. M., Sep 2000. Measuring the thickness of the human cerebral cortex from magnetic resonance images. Proc Natl Acad Sci U S A 97 (20), 11050–5.

[26] Fischl, B., Salat, D. H., Busa, E., Albert, M., Dieterich, M., Haselgrove, C., van der Kouwe, A., Killiany, R., Kennedy, D., Klaveness, S., Montillo, A., Makris, N., Rosen, B., Dale, A. M., Jan 2002. Whole brain segmentation: automated labeling of neuroanatomical structures in the human brain. Neuron 33 (3), 341–55.

[27] Fischl, B., Sereno, M. I., Dale, A. M., Feb 1999. Cortical surface-based analysis. ii: Inflation, flattening, and a surface-based coordinate system. Neuroimage 9 (2), 195–207.

[28] Fischl, B., van der Kouwe, A., Destrieux, C., Halgren, E., Ségonne, F., Salat, D. H., Busa, E., Seidman, L. J., Goldstein, J., Kennedy, D., Caviness, V., Makris, N., Rosen, B., Dale, A. M., Jan 2004. Automatically parcellating the human cerebral cortex. Cereb Cortex 14 (1), 11–22.

[29] Fortier, C. B., Leritz, E. C., Salat, D. H., Venne, J. R., Maksimovskiy, A. L., Williams, V., Milberg, W. P., McGlinchey, R. E., Dec 2011. Reduced cortical thickness in abstinent alcoholics and association with alcoholic behavior. Alcohol Clin Exp Res 35 (12), 2193–201.

[30] Foster, N. E. V., Zatorre, R. J., Oct 2010. Cortical structure predicts success in performing musical transformation judgments. Neuroimage 53 (1), 26–36.

[31] Gernsbacher, M. A., Jan 2007. Presidential column: The eye of the beholder. Observer 20 (1).

[32] Haier, R. J., Karama, S., Leyba, L., Jung, R. E., 2009. MRI assessment of cortical thickness and functional activity changes in adolescent girls following three months of practice on a visual-spatial task. BMC Res Notes 2, 174.

[33] Hardan, A. Y., Muddasani, S., Vemulapalli, M., Keshavan, M. S., Minshew, N. J., Jul 2006. An MRI study of increased cortical thickness in autism. Am J Psychiatry 163 (7), 1290–2.

[34] He, Y., Chen, Z. J., Evans, A. C., Oct 2007. Small-world anatomical networks in the human brain revealed by cortical thickness from MRI. Cereb Cortex 17 (10), 2407–19.

[35] Jones, S. E., Buchbinder, B. R., Aharon, I., Sep 2000. Three-dimensional mapping of cortical thickness using Laplace's equation. Hum Brain Mapp 11 (1), 12–32.

[36] Jubault, T., Gagnon, J.-F., Karama, S., Ptito, A., Lafontaine, A.-L., Evans, A. C., Monchi, O., Mar 2011. Patterns of cortical thickness and surface area in early Parkinson's disease. Neuroimage 55 (2), 462–7.

[37] Kim, J. S., Singh, V., Lee, J. K., Lerch, J., Ad-Dab'bagh, Y., MacDonald, D., Lee, J. M., Kim, S. I., Evans, A. C., Aug 2005. Automated 3-D extraction and evaluation of the inner and outer cortical surfaces using a Laplacian map and partial volume effect classification. Neuroimage 27 (1), 210–21.

[38] Klein, A., Ghosh, S. S., Avants, B., Yeo, B. T. T., Fischl, B., Ardekani, B., Gee, J. C., Mann, J. J., Parsey, R. V., May 2010. Evaluation of volume-based and surface-based brain image registration methods. Neuroimage 51 (1), 214–20.

[39] Kochunov, P., Glahn, D. C., Lancaster, J., Thompson, P. M., Kochunov, V., Rogers, B., Fox, P., Blangero, J., Williamson, D. E., Sep 2011. Fractional anisotropy of cerebral white matter and thickness of cortical gray matter across the lifespan. Neuroimage 58 (1), 41–9.

[40] Kovacevic, J., 2006. From the editor-in-chief. IEEE Trans Imag Process 15 (12).

[41] Kühn, S., Schubert, F., Gallinat, J., Dec 2010. Reduced thickness of medial orbitofrontal cortex in smokers. Biol Psychiatry 68 (11), 1061–5.

[42] Lerch, J. P., Worsley, K., Shaw, W. P., Greenstein, D. K., Lenroot, R. K., Giedd, J., Evans, A. C., Jul 2006. Mapping anatomical correlations across cerebral cortex (MACACC) using cortical thickness from MRI. Neuroimage 31 (3), 993–1003.

[43] Luders, E., Narr, K. L., Thompson, P. M., Rex, D. E., Jancke, L., Toga, A. W., Aug 2006. Hemispheric asymmetries in cortical thickness. Cereb Cortex 16 (8), 1232–8.

[44] Luders, E., Narr, K. L., Thompson, P. M., Rex, D. E., Woods, R. P., Deluca, H., Jancke, L., Toga, A. W., Apr 2006. Gender effects on cortical thickness and the influence of scaling. Hum Brain Mapp 27 (4), 314–24.

[45] Lyoo, I. K., Sung, Y. H., Dager, S. R., Friedman, S. D., Lee, J.-Y., Kim, S. J., Kim, N., Dunner, D. L., Renshaw, P. F., Feb 2006. Regional cerebral cortical thinning in bipolar disorder. Bipolar Disord 8 (1), 65–74.

[46] MacDonald, D., Kabani, N., Avis, D., Evans, A. C., Sep 2000. Automated 3-D extraction of inner and outer surfaces of cerebral cortex from MRI. Neuroimage 12 (3), 340–56.

[47] Magnotta, V. A., Andreasen, N. C., Schultz, S. K., Harris, G., Cizadlo, T., Heckel, D., Nopoulos, P., Flaum, M., Mar 1999. Quantitative in vivo measurement of gyrification in the human brain: changes associated with aging. Cereb Cortex 9 (2), 151–60.

[48] Makris, N., Gasic, G. P., Kennedy, D. N., Hodge, S. M., Kaiser, J. R., Lee, M. J., Kim, B. W., Blood, A. J., Evins, A. E., Seidman, L. J., Iosifescu, D. V., Lee, S., Baxter, C., Perlis, R. H., Smoller, J. W., Fava, M., Breiter, H. C., Oct 2008. Cortical thickness abnormalities in cocaine addiction–a reflection of both drug use and a pre-existing disposition to drug abuse? Neuron 60 (1), 174–88.

[49] Mazziotta, J. C., Toga, A. W., Evans, A., Fox, P., Lancaster, J., Jun 1995. A probabilistic atlas of the human brain: theory and rationale for its development. the International Consortium for Brain Mapping (ICBM). Neuroimage 2 (2), 89–101.

[50] Nesvåg, R., Lawyer, G., Varnäs, K., Fjell, A. M., Walhovd, K. B., Frigessi, A., Jönsson, E. G., Agartz, I., Jan 2008. Regional thinning of the cerebral cortex in schizophrenia: effects of diagnosis, age and antipsychotic medication. Schizophr Res 98 (1-3), 16–28.

[51] Otsu, N., 1979. A threshold selection method from gray-level histograms. EEE Trans. Sys., Man., Cyber. 9 (1), 62–66.

[52] Peterson, B. S., Warner, V., Bansal, R., Zhu, H., Hao, X., Liu, J., Durkin, K., Adams, P. B., Wickramaratne, P., Weissman, M. M., Apr 2009. Cortical thinning in persons at increased familial risk for major depression. Proc Natl Acad Sci U S A 106 (15), 6273–8.

[53] Raine, A., Laufer, W. S., Yang, Y., Narr, K. L., Thompson, P., Toga, A. W., Oct 2011. Increased executive functioning, attention, and cortical thickness in white-collar criminals. Hum Brain Mapp.

[54] Raji, C. A., Ho, A. J., Parikshak, N. N., Becker, J. T., Lopez, O. L., Kuller, L. H., Hua, X., Leow, A. D., Toga, A. W., Thompson, P. M., Mar 2010. Brain structure and obesity. Hum Brain Mapp 31 (3), 353–64.

[55] Ramasamy, D. P., Benedict, R. H. B., Cox, J. L., Fritz, D., Abdelrahman, N., Hussein, S., Minagar, A., Dwyer, M. G., Zivadinov, R., Jul 2009. Extent of cerebellum, subcortical and cortical atrophy in patients with MS: a case-control study. J Neurol Sci 282 (1-2), 47–54.

[56] Rosas, H. D., Hevelone, N. D., Zaleta, A. K., Greve, D. N., Salat, D. H., Fischl, B., Sep 2005. Regional cortical thinning in preclinical Huntington disease and its relationship to cognition. Neurology 65 (5), 745–7.

[57] Rosas, H. D., Liu, A. K., Hersch, S., Glessner, M., Ferrante, R. J., Salat, D. H., van der Kouwe, A., Jenkins, B. G., Dale, A. M., Fischl, B., Mar 2002. Regional and progressive thinning of the cortical ribbon in Huntington's disease. Neurology 58 (5), 695–701.

[58] Scott, M. L. J., Bromiley, P. A., Thacker, N. A., Hutchinson, C. E., Jackson, A., Apr 2009. A fast, model-independent method for cerebral cortical

thickness estimation using MRI. Med Image Anal 13 (2), 269–85.
[59] Ségonne, F., Dale, A. M., Busa, E., Glessner, M., Salat, D., Hahn, H. K., Fischl, B., Jul 2004. A hybrid approach to the skull stripping problem in MRI. Neuroimage 22 (3), 1060–75.
[60] Selemon, L. D., Rajkowska, G., Goldman-Rakic, P. S., Jan 2004. Evidence for progression in frontal cortical pathology in late-stage Huntington's disease. J Comp Neurol 468 (2), 190–204.
[61] Shattuck, D. W., Mirza, M., Adisetiyo, V., Hojatkashani, C., Salamon, G., Narr, K. L., Poldrack, R. A., Bilder, R. M., Toga, A. W., Feb 2008. Construction of a 3D probabilistic atlas of human cortical structures. Neuroimage 39 (3), 1064–80.
[62] Shattuck, D. W., Sandor-Leahy, S. R., Schaper, K. A., Rottenberg, D. A., Leahy, R. M., May 2001. Magnetic resonance image tissue classification using a partial volume model. Neuroimage 13 (5), 856–76.
[63] Shaw, P., Greenstein, D., Lerch, J., Clasen, L., Lenroot, R., Gogtay, N., Evans, A., Rapoport, J., Giedd, J., Mar 2006. Intellectual ability and cortical development in children and adolescents. Nature 440 (7084), 676–9.
[64] Shin, Y.-W., Yoo, S. Y., Lee, J. K., Ha, T. H., Lee, K. J., Lee, J. M., Kim, I. Y., Kim, S. I., Kwon, J. S., Nov 2007. Cortical thinning in obsessive compulsive disorder. Hum Brain Mapp 28 (11), 1128–35.
[65] Sled, J. G., Zijdenbos, A. P., Evans, A. C., Feb 1998. A nonparametric method for automatic correction of intensity nonuniformity in MRI data. IEEE Trans Med Imaging 17 (1), 87–97.
[66] Smith, S. M., Nov 2002. Fast robust automated brain extraction. Hum Brain Mapp 17 (3), 143–55.
[67] Smith, S. M., Jenkinson, M., Woolrich, M. W., Beckmann, C. F., Behrens, T. E. J., Johansen-Berg, H., Bannister, P. R., De Luca, M., Drobnjak, I., Flitney, D. E., Niazy, R. K., Saunders, J., Vickers, J., Zhang, Y., De Stefano, N., Brady, J. M., Matthews, P. M., 2004. Advances in functional and structural MR image analysis and implementation as FSL. Neuroimage 23 Suppl 1, S208–19.
[68] Sowell, E. R., Kan, E., Yoshii, J., Thompson, P. M., Bansal, R., Xu, D., Toga, A. W., Peterson, B. S., Jun 2008. Thinning of sensorimotor cortices in children with Tourette syndrome. Nat Neurosci 11 (6), 637–9.
[69] Talairach, J., Tournoux, P., 1988. Co-planar stereotaxic atlas of the human brain: 3-Dimensional proportional system—An approach to cerebral imaging. Thieme.
[70] Thompson, P. M., Lee, A. D., Dutton, R. A., Geaga, J. A., Hayashi, K. M., Eckert, M. A., Bellugi, U., Galaburda, A. M., Korenberg, J. R., Mills, D. L., Toga, A. W., Reiss, A. L., Apr 2005. Abnormal cortical complexity and thickness profiles mapped in williams syndrome. J Neurosci 25 (16), 4146–58.
[71] Tustison, N. J., Avants, B. B., Cook, P. A., Zheng, Y., Egan, A., Yushkevich, P. A., Gee, J. C., Jun 2010. N4ITK: improved N3 bias correction. IEEE Trans Med Imaging 29 (6), 1310–20.
[72] Vachet, C., Hazlett, H. C., Niethammer, M., Oguz, I., Cates, J., Whitaker, R., Piven, J., Styner, M., February 2011. Group-wise automatic mesh-based analysis of cortical thickness. In: Benoit M. Dawant, D. R. H. (Ed.), SPIE Medical Imaging: Image Processing.
[73] Wang, D., Shi, L., Chu, W. C. W., Burwell, R. G., Cheng, J. C. Y., Ahuja, A. T., Jan 2012. Abnormal cerebral cortical thinning pattern in adolescent girls with idiopathic scoliosis. Neuroimage 59 (2), 935–42.
[74] Ward, B. D., 1999. Intracranial segmentation. Tech. rep., Medical College of Wisconsin, http://afni.nimh.nih.gov/pub/dist/doc/3dIntracranial.pdf.
[75] Wei, G., Zhang, Y., Jiang, T., Luo, J., 2011. Increased cortical thickness in sports experts: a comparison of diving players with the controls. PLoS One 6 (2), e17112.
[76] Worsley, K. J., Chen, J.-I., Lerch, J., Evans, A. C., May 2005. Comparing functional connectivity via thresholding correlations and singular value decomposition. Philos Trans R Soc Lond B Biol Sci 360 (1457), 913–20.
[77] Yezzi, Jr, A. J., Prince, J. L., Oct 2003. An Eulerian PDE approach for computing tissue thickness. IEEE Trans Med Imaging 22 (10), 1332–9.
[78] Zeng, X., Staib, L. H., Schultz, R. T., Duncan, J. S., Oct 1999. Segmentation and measurement of the cortex from 3-D MR images using coupled-surfaces propagation. IEEE Trans Med Imaging 18 (10), 927–37.
[79] Zhang, Y., Brady, M., Smith, S., Jan 2001. Segmentation of brain MR images through a hidden Markov random field model and the expectation-maximization algorithm. IEEE Trans Med Imaging 20 (1), 45–57.
[80] Zubiaurre-Elorza, L., Junque, C., Gómez-Gil, E., Segovia, S., Carrillo, B., Rametti, G., Guillamon, A., 2012. Cortical thickness in untreated transsexuals. Cerebral Cortex.